Construction of Size-Controllable Hierarchical Nanoporous TiO_2 Ring Arrays and Their Modifications

Fengqiang Sun, Jimmy C. Yu,* and Xinchen Wang

Department of Chemistry and the Center of Novel Functional Molecules, The Chinese University of Hong Kong, Shatin, New Territories, Hong Kong, People's Republic of China

Received April 27, 2006. Revised Manuscript Received June 11, 2006

TiO_2 hierarchical nanoporous ring arrays are constructed on a solid surface by an annealed template-induced sol-soaking strategy. The ring size can be controlled by changing the sol concentration and varying the annealing time of the polystyrene sphere colloidal monolayer. The sol−gel process generates porous nanocrystalline networks in the ring walls, which can be modified by incorporating functional particles into the pores. This strategy allows the fabrication of specific metal oxides and semiconductor ring arrays on both flat and curved surfaces.

Introduction

Ring-like structures have recently received much attention because of their unique properties and applications in magnetic,[1,2] optical,[3,4] and opto-electronic devices.[5] These properties are usually size-dependent. For example, gold rings exhibit tunable localized Plasmon resonance in the near-infrared spectrum by varying their size. The development of methods that allow easy control of the ring size is, therefore, highly desirable. Interesting properties can also be obtained and controlled by modifying the as-synthesized rings with functional materials.[6] Another factor that influences the properties is the ultrafine structure of the ring walls, but there are few related reports. Generally speaking, ring walls with nanopores can be easily modified to enhance their functions. The control of ring size and the introduction of nanopores into the ring walls are important means for the design of new functional materials.

Ring structures can be fabricated by photolithography,[4] electrobeam lithography,[7] and molecular-beam epitaxy (MBE) methods.[8] However, these methods are usually expensive and time-consuming and can be limited in resolution. An alternative approach, namely, the template-induced technique, has become attractive in synthesizing mesoscopic ring arrays. The templates are usually ordered pore arrays,[9−15] nonclosely arranged latex spheres,[3,16,17] and three-dimensional colloidal crystals.[18,19] A colloidal monolayer, as a kind of colloidal crystal, is a flexible template used in synthesizing ordered porous films[20] or periodical particle arrays.[21] Recently, it has been used to synthesize ring arrays by colloidal suspension deposition,[22] solution dipping,[23,24] physical vapor deposition,[25,26] and selective etching methods.[10,27] Their ring sizes can be controlled by using templates of different dimensions; once the sizes are changed, the center-to-center (CTC) spacing between adjacent rings will be changed naturally. Although Yi and Kim[10] could control the ring size and maintain the CTC spacing, different types of templates for pores and rings must be employed. Consequently, the shapes of their ring structures were somewhat irregular. It is still

* To whom correspondence should be addressed. E-mail: jimyu@cuhk.edu.hk.

(1) Mailly, D.; Chaperlier, C.; Benoit, A. *Phys. Rev. Lett.* **1993**, *70*, 2020−2023.
(2) Rabaud, W.; Saminadayar, L.; Mailly, D.; Hasselbach, K.; Benoit, A.; Etienne, B. *Phys. Rev. Lett.* **2001**, *86*, 3124−3127.
(3) Aizpurua, J.; Hanarp, P.; Sutherland, D. S.; Käll, M.; Bryant, G. W.; García de Abajo, F. J. *Phys. Rev. Lett.* **2003**, *90*, 057401.
(4) Warburton, R. J.; Schäflein, C.; Haft, D.; Bickel, F.; Lorke, A.; Karrai, K.; Garcia, J. M.; Schoenfeld, W.; Petroff, P. M. *Nature* **2000**, *405*, 926−929.
(5) Choi, H. W.; Jeon, C. W.; Liu, C.; Watson, I. M.; Dawson, M. D.; Edwards, P. R.; Martin, R. W.; Tripathy, S.; Chua, S. J. *Appl. Phys. Lett.* **2005**, *86*, 21101.
(6) Wang, Y.; Han, S. B.; Briseno, A. L.; Sanedrin, R. J. G.; Zhou, F. M. *J. Mater. Chem.* **2004**, *14*, 3488−3494.
(7) Brands, M.; Carl, A.; Dumpich, G. *Superlattices Microstruct.* **2005**, *37*, 388−393.
(8) Granados, D.; García, J. M. *Appl. Phys. Lett.* **2003**, *82*, 2401−2403.
(9) Lu, G.; Li, W.; Yao, J. M.; Zhang, G.; Yang, B.; Shen, J. C. *Adv. Mater.* **2002**, *14*, 1049−1053.
(10) Yi, D. K.; Kim, D. Y. *Nano Lett.* **2003**, *3*, 207−211.
(11) Xu, H.; Goedel, W. A. *Angew. Chem., Int. Ed.* **2003**, *42*, 4696−4700.
(12) Yan, F.; Goedel, W. A. *Nano Lett.* **2004**, *4*, 1193−1196.
(13) Hobbs, K. L.; Larson, P. R.; Lian, G. D.; Keay, J. C.; Johnson, M. B. *Nano Lett.* **2004**, *4*, 167−171.
(14) Wang, Z. K.; Lim, H. S.; Liu, H. Y.; Ng, S. C.; Kuok, M. H. *Phys. Rev. Lett.* **2005**, *94*, 137208.
(15) Pearson, D. H.; Tonucci, R. J.; Bussmann, K. M.; Bolden, E. A. *Adv. Mater.* **1999**, *11*, 769−773.
(16) Zhu, F. Q.; Fan, D. L.; Zhu, X. C.; Zhu, J. G.; Cammarata, R. C.; Chien, C. L. *Adv. Mater.* **2004**, *16*, 2155−2159.
(17) McLellan, J. M.; Geissler, M.; Xia, Y. N. *J. Am. Chem. Soc.* **2004**, *126*, 10830−10831.
(18) Chen, X.; Chen, Z. M.; Fu, N.; Lu, G.; Yang, B. *Adv. Mater.* **2003**, *15*, 1413−1417.
(19) Yan, F.; Goedel, W. A. *Angew. Chem., Int. Ed.* **2005**, *44*, 2084−2088.
(20) Matsushita, S. I.; Miwa, T.; Tryk, D. A.; Fujishima, A. *Langmuir* **1998**, *14*, 6441−6447.
(21) Hulteen, J. C.; Treichel, D. A.; Smith, M. T.; Duval, M. L.; Jensen, T. R.; Van Duyne, R. P. *J. Phys. Chem. B* **1999**, *103*, 3854−3863.
(22) Tessier, P. M.; Velev, O. D.; Kalambur, A. T.; Lenhoff, A. M.; Rabolt, J. F.; Kaler, E. W. *Adv. Mater.* **2001**, *13*, 396−400.
(23) Boneberg, J.; Burmeister, F.; Schäfle, C.; Leiderer, P. *Langmuir* **1997**, *13*, 7080−7084.
(24) Sun, F. Q.; Cai, W. P.; Li, Y.; Cao, B. Q.; Lei, Y.; Zhang, L. D. *Adv. Funct. Mater.* **2004**, *14*, 283−288.
(25) Winzer, M.; Kleiber, M.; Dix, N.; Wiesendanger, R. *Appl. Phys. A* **1996**, *63*, 617−619.
(26) Kosiorek, A.; Kandulski, W.; Glaczynska, H.; Giersig, M. *Small* **2005**, *1*, 439−444.
(27) Marczewski, D.; Goedel, W. A. *Nano Lett.* **2005**, *5*, 295−299.

10.1021/cm060982s CCC: $33.50
Published on Web 07/08/2006

difficult to fabricate rings of specific size and arrays of high uniformity (e.g., size-tunable rings with specific CTC spacing). Moreover, the rings prepared by conventional methods do not possess hierarchical structures, and they cannot be modified easily.

It is known that the contact area between a polystyrene sphere (PS) colloidal monolayer and a substrate changes during heat treatment.[28] When rings evolve around heated spheres, the ring size changes with temperature but the spacing between the rings always remains the same. The development of methods for introducing the ring materials is another technical issue to be considered. Matsushita et al. prepared macropore arrays by soaking the colloidal monolayer into solutions using a spray process.[29] In this paper, we present an alternative strategy (annealed template-induced sol soaking) to synthesize size-controllable TiO_2. It is also possible to obtain nanoporous structures in the pore walls by employing appropriate sols as precursors.[30,31]

TiO_2 was used as a model material, because it possesses good photocatalytic, optical, gas-sensing, and electronic properties. Although there were several reports on TiO_2 ring systems, those rings were not arranged in an orderly manner[19] or it was difficult if not impossible to control the ring size and obtain nanoporous structures in the ring walls. The method described here allows the fabrication of TiO_2 into a discrete and ordered ring array system. The ring walls are composed of nanoporous TiO_2 and possess high specific surface area. Noble metal particles can be easily incorporated into the nanopores by a photocatalysis process, thus allowing the design of composite ring arrays with attractive catalytic properties. Interestingly, if the colloidal monolayer is transferred onto a curved surface[32] before applying this strategy, we would be able to fabricate ring arrays directly on such a surface. The as-prepared and noble metal loaded ring arrays might be used in optoelectronic devices, photocatalytic systems, and gas sensors.

Experimental Section

Preparation of Colloidal Monolayers and TiO_2 Sols. Ordinary glass slides were washed in turn with ethanol, 3:1 98% H_2SO_4/H_2O_2, 5:1:1 H_2O/NH_3·H_2O/H_2O_2, and distilled water. Monodispersed 4.5 μm PS suspensions (2.5 wt % in water, surfactant-free) were obtained from Alfa Aesar Corporation. A drop (~20 μL) of the suspension was pipetted onto a glass slide mounted in a custom-built spin coater. Then a large area (more than 1 cm^2) of colloidal monolayer was synthesized with the spin-coating method.[21] The spinning speed was 80 rev/min.

The TiO_2 sol was synthesized by acid hydrolysis of titanium isopropoxide. Detailed preparation procedures for the sol can be found elsewhere.[33]

Preparation of Nanoporous TiO_2 Rings. As shown in Scheme 1, a PS colloidal monolayer was chosen as the original template.

Scheme 1. Annealed Template-Induced Sol-Soaking Strategy for Synthesizing Ordered Ring Arrays[a]

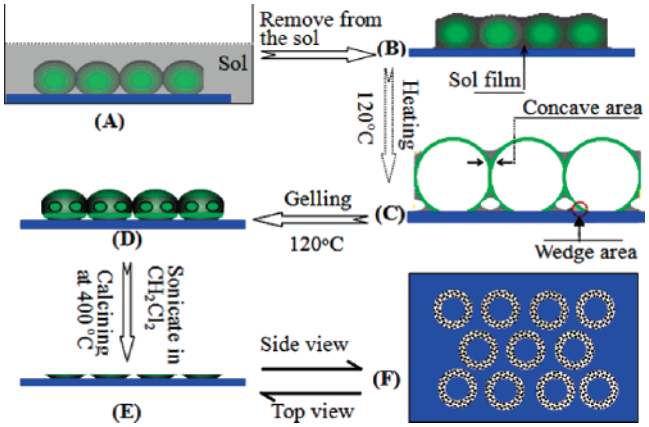

[a] (A) Annealed PS colloidal monolayer soaked in the sol; (B) colloidal monolayer with the sol in the interstices; (C) a profile view of the colloidal monolayer and the sol film divided two layers; (D) a lateral view of the colloidal monolayer and gel shells; (E) a lateral view of the ring arrays; and (F) top view of the nanoporous ring arrays.

As the first step, the glass substrate covered with PS was put into an oven and annealed at 120 °C. The colloidal monolayer binded to the substrate, and plane contacts were formed between the spheres and the substrate.[28] The annealed sample was then soaked into the TiO_2 sol for at least 30 min (A). The monolayer was removed from the sol, and the excess sol on the surface of the colloidal monolayer was removed with a ChemWipe. The sol filled the interstices between the spheres and could be regarded as a film coated on the colloidal monolayer (B). The sample was put into the oven again and heated at 120 °C for 1 h. During this process, the sol film ruptured and divided into two layers: the first layer was in the wedge area formed by the PSs and the substrate; the other layer was in the concave areas formed by two adjacent spheres and the triangle interstices among three closely packed spheres (C). The two-layer sols then gelled around the spheres independently (D). The TiO_2 colloid nanoparticles piled up in the gel, and nanoporous structures were formed in the layers.[34] Finally the sample was sonicated in dichloromethane for about 1 h. PSs and the upper layer were removed, and specifically sized mesoscopic ring arrays were left on the substrate (E and F). After calcination at 400 °C for 2 h, uniform ring arrays with nanopores in the walls were obtained. The ring size could be controlled by the sol concentration and annealing time of the colloidal monolayer.

As a control experiment, a TiO_2 thin film was prepared from 10 mL of the TiO_2 sol in a Petri dish. Because the thin film was fabricated from the same sol under identical heat-treatment conditions as that for the rings, it was used for the measurement of the nanopore size distribution and specific surface area of both TiO_2 nanoporous structures.[35]

Loading the Silver and Gold Particles into the Nanopores. The precursor solutions of silver and gold were 0.05 M $AgNO_3$ and 0.02 M $HAuCl_4$, respectively. The as-synthesized nanoporous TiO_2 ring array was immerged in a flask filled with the precursor. The bottle was placed in an ultrasonic bath and connected to a vacuum pump. After sonication under reduced air pressure for 5−10 min, the ring array was washed with deionized water. And then it was irradiated with UV light (254 nm, 10 mW cm^{-2}) in the presence of methanol vapor for 4 h to obtain noble metal particle-loaded TiO_2 ring arrays by photochemical deposition.[35]

(28) Sun, F. Q.; Cai, W. P.; Li, Y.; Cao, B. Q.; Lu, F.; Duan, G. T.; Zhang, L. D. *Adv. Mater.* **2004**, *16*, 1116−1121.
(29) Matsushita, S.; Miwa, T.; Fujishima, A. *Chem. Lett.* **1997**, *309*, 925−926.
(30) Tian, Y.; Tatsuma, T. *Chem. Commun.* **2004**, *16*, 1810−1812.
(31) Sures Singh, R.; Grimes, C. A.; Dickey, E. C. *Mater. Res. Innovations* **2002**, *5*, 178−184.
(32) Sun, F. Q.; Cai, W. P.; Li, Y.; Jia, L. C.; Lu, F. *Adv. Mater.* **2005**, *17*, 2872−2877.
(33) Xu, Q. Y.; Anderson, M. A. *J. Mater. Res.* **1991**, *6*, 1073−1079.
(34) Jin, Z. H.; Zhou, H. J.; Jin, Z. L.; Savinell, R. F.; Liu, C. C. *Sens. Actuators, B* **1998**, *52*, 188−194.
(35) Yu, J. C.; Wang, X. C.; Wu, L.; Ho, W. K.; Zhang, L. Z.; Zhou, G. T. *Adv. Funct. Mater.* **2004**, *14*, 1178−1183.

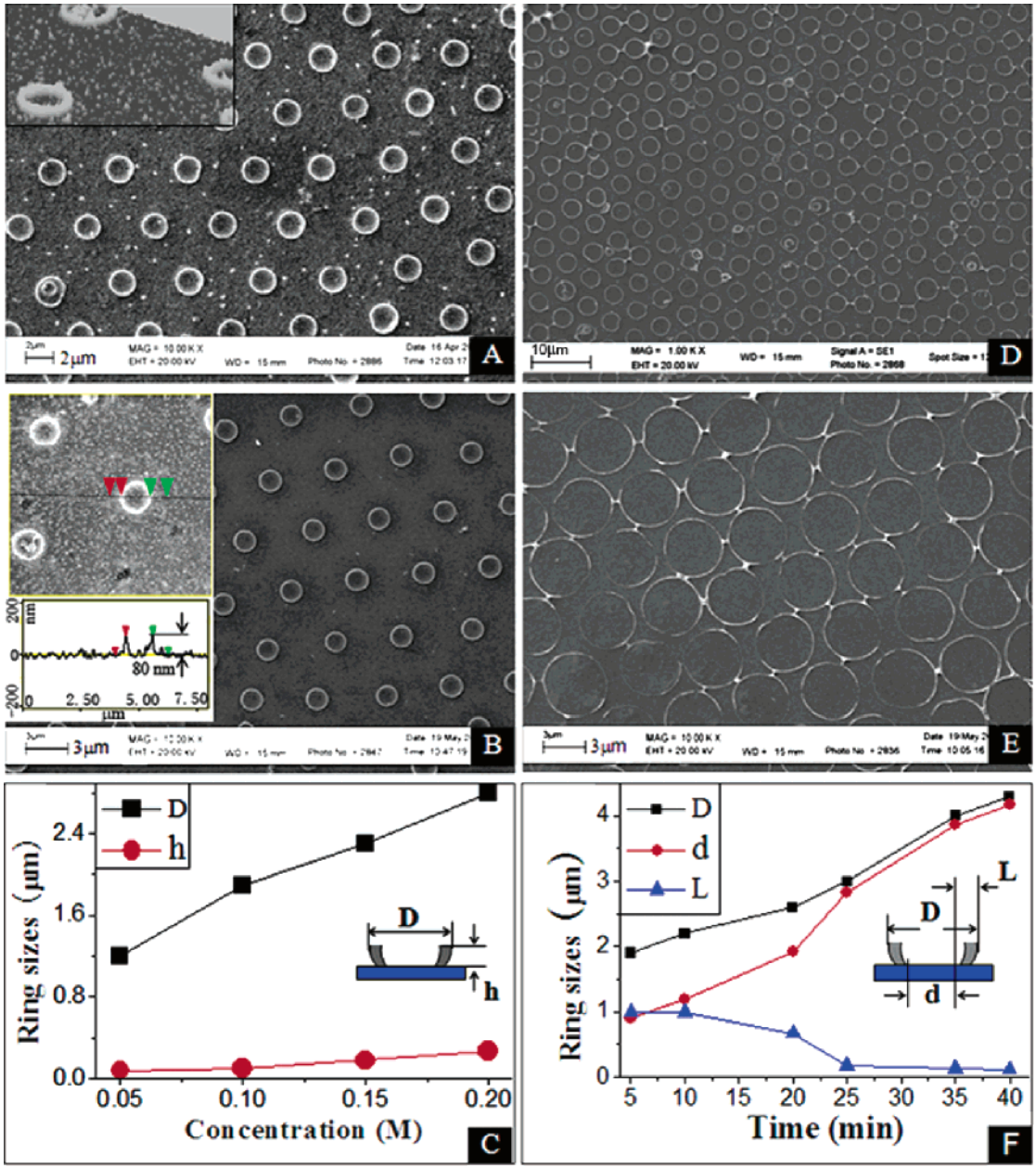

Figure 1. SEM images of sizes-varied TiO_2 ring arrays and size statistics. Templates (4.5 μm PS colloidal monolayer) of A and B were both annealed for 5 min at 120 °C but with 0.1 M and 0.05 M of TiO_2 sols, respectively. The concentration of the TiO_2 sol in parts A, D, and E was 0.1 M, but the annealing times were 5, 25, and 40 min, respectively. Part C shows the ring size statistics of a series of samples similar to A and B; F is that for a series of samples similar to A, E, and F.

Characterizations. Scanning electron microscopy (SEM) images were recorded on a LEO 1450VP scanning electron microscope. The N_2-sorption isotherm was recorded at 77 K using a micrometritics ASAP 2010 instrument using samples scratched off the bottom of the Petri dish. The UV−vis optical absorption curves were recorded on Cary 100 UV−visible spectrophotometer.

Results and Discussion

Figure 1 shows the SEM images of the TiO_2 mesoscopic ring arrays of different sizes. X-ray diffraction (XRD) patterns (not shown here) confirm that the rings mainly consist of anatase-phased TiO_2. All rings are bowl-like, as shown in the inset of Figure 1C. They are arranged hexagonally, and the distance between two adjacent ring centers is always equal to the diameter of the PS. By varying the concentration of precursor or the annealing time of colloidal monolayers, the outer diameter, the height, the inner diameter, and the ring-wall thickness can be readily controlled. Figure 1A,B was acquired from 0.1 and 0.05 M, TiO_2 sols, and all the colloidal monolayers were heated for 5 min at 120 °C. The inset in Figure 1A is a three-dimensional view of the corresponding atomic force microscopy (AFM) image, which clearly shows the ring structure. The height of the rings can be estimated from the AFM image as shown in the inset of Figure 1B. The inner diameters of all rings are around 0.8 μm, while the outer diameters and the heights vary according to the concentration of the precursor. Such a concentration dependency is shown in Figure 1C. When the concentration is increased from 0.05 to 0.2 M, the outer diameter increases from 1.2 to 2.8 μm, and the corresponding height changes from 80 to around 270 nm. The annealing treatment of the colloidal monolayer also influences the ring

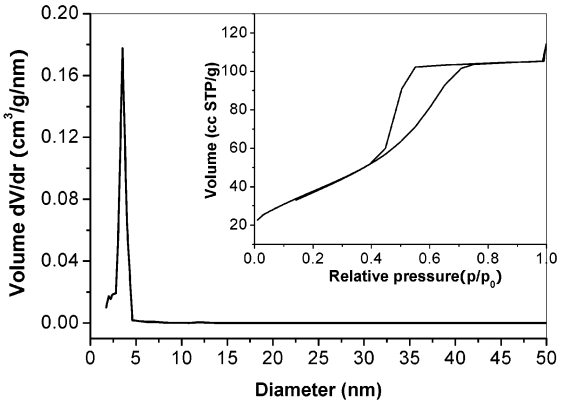

Figure 2. Pore-size distribution and N_2 adsorption−desorption isotherms (inset) for the nanoporous TiO_2 film prepared under the same heat-treatment condition as that of the ring arrays.

size, as shown in Figure 1A,D,E,F, where the concentration remains constant at 0.1 M but the annealing time is changed from 5 to 40 min. Figure 1F summarizes the dependency on annealing time. The inner diameter increases gradually from 0.8 μm to 4.2 μm with an increase in annealing time. Correspondingly, the outer diameter is increased from 2.0 μm to 4.3 μm, while the thickness of the ring walls decreases from 600 to about 60 nm. The distances between the adjacent ring walls gradually decrease as the heating time is increased up to 40 min, at which time the rings are nearly connected with each other.

The rings should have the same porous structure as a TiO_2 film prepared under identical heat-treatment conditions.[35] As shown in Figure 2, a film prepared on a Petri dish has a high Brunauer−Emmett−Teller (BET) surface area of about 138 m^2/g (calculated from the linear part of the BET plot ($P/P_0 = 0.1-0.2$)). The total pore volume is 0.183 cm^3/g (taken from the volume of N_2 adsorbed at $P/P_0 = 0.995$). The N_2 sorptions are found to be type-IV isotherm, typical of a mesoporous structure solid. It shows a narrow pore-size distribution of ~3.5 nm.

Figure 3 describes the ring formation mechanism. Once a colloidal monolayer is formed on the substrate, there are many periodical interstices between the monolayer and the substrate (Figure 3A). There are wedge areas between the PS and the substrate and also concave areas between adjacent spheres. These wedge and concave areas are areas which can produce capillary forces when they are filled with sols. A suitable anneal treatment not only binds the plastic PSs onto the substrate but also deforms them in situ, which provides plane contacts between the PSs and the substrate and between the two adjacent spheres. Such characteristics are required for the ring formation.

The substrate surface and latex spheres are hydrophilic and thus allow positive capillary action[9,18] on the sol. The sol fills in the interstices and forms a meniscus between two adjacent spheres because of the capillary action, as shown in Figure 3B. Upon heating at 120 °C, the sol film coated on the spheres undergoes several physical changes. Water is evaporated gradually from the top and the edges of the colloidal monolayer. The continuous evaporation (the flux j_{ev} and j_{eh}) makes the surface and the edge of the colloidal monolayer in an atmosphere unsaturated with water vapor.

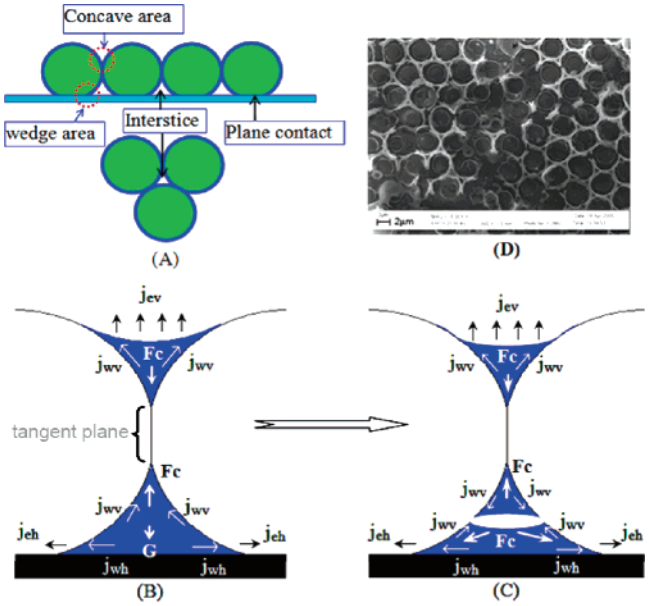

Figure 3. Formation process of ring arrays. (A) A schematic illustration of the microstructures of the annealed colloidal monolayer on the substrate; (B) state when the sample starts to be heated; (C) state when the sol film ruptures; and (D) state (SEM image) after the sol gels and spheres are removed with dichloromethane. j_{ev} and j_{eh} are the vertical and horizontal water evaporation fluxes, respectively; j_{wv} and j_{wh} are the vertical and horizontal water influx respectively; F_c is the capillary force; and G is gravitation.

This leads to pressure gradients (ΔP)[36] in the vertical and the horizontal directions. The pressure gradient produces water influxes from the bulk sol in the interstices toward the surface (j_{wv}) and the edge (j_{wh}) of the sol film. At the same time, the sol is affected by the capillary force (F_c) produced by the concave areas between the adjacent spheres and will have a tendency to move to these areas. The sol below the tangent plane suffers an upward pull because of the capillary force. Besides, the sol is also affected by the downward gravitation (G), though it may be ignored in the micro-/nanometer scale comparing with the capillary force. Under these physical actions, the sol film goes through changes in three stages. (i) The liquid surface above the colloidal monolayer is slightly lowered, and the sol is condensed. (ii) As the quantity of water decreases, the combined action of all forces and influxes in different directions causes the sol film to rupture upon heating, starting from a point in the special microspace between the colloidal monolayer and the substrate. Therefore, the sol is divided into two layers, as shown in Figure 3C. The bottom sol film is very thin and ruptures again due to water influxes and capillary force. The ruptured sol films then move toward the contact lines between PSs and the substrate to form independent sol rings around PSs (Scheme 1C). (iii) The upper sol forms an ordered porous film (Scheme 1D), whereas the bottom sol forms ring arrays. The TiO_2 colloidal particles in the sols bring together a kind of disordered mesoporous structure in the pore and ring walls.[37] Upon dissolving the PSs in dichloromethane (without sonication), the upper ordered porous film falls down onto the substrate. This results in the formation of a two-layer structure, as

(36) Dimitrov, A. S.; Nagayama, K. *Langmuir* **1996**, *12*, 1303−1311.
(37) Longo, C.; De Paoli, M. A. *J. Braz. Chem. Soc.* **2003**, *14*, 889−901.

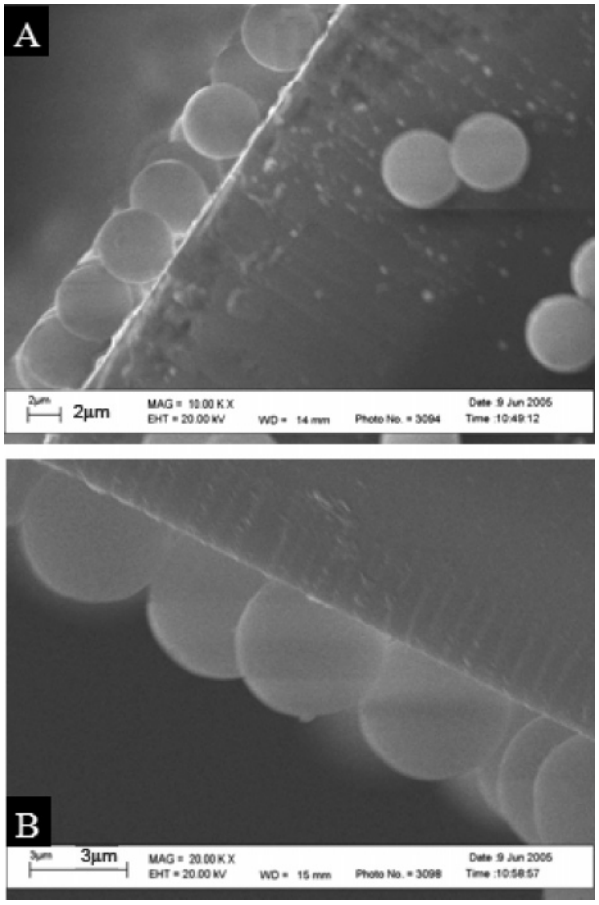

Figure 4. Side views (SEM) of annealed 4.5 μm PS colloidal monolayers on a flat substrate. The annealing times at 120 °C were (A) 5 min and (B) 35 min.

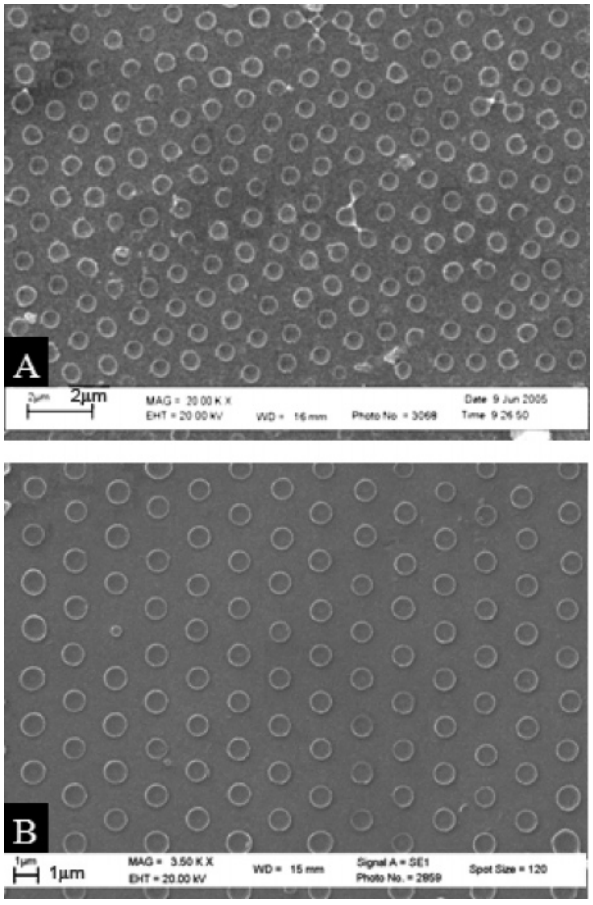

Figure 5. TiO_2 ring arrays synthesized with 1.0 μm (A) and 2.0 μm (B) PS colloidal monolayers. The templates were annealed for 5 min at 120 °C; the concentrations of the TiO_2 sol were 0.02 M and 0.05 M, respectively.

shown in Figure 3D. If sonication is applied, the upper layer is removed and only the nanoporous ring array is left on the substrate. Because of the anneal-induced in situ deformation, the plastic PSs become truncated oblate spheres. The contact plane between the sphere and the substrate is circular,[3,28] which is essential for the ring formation. The ring grows around the oblate template and shows a bowl-like arrangement (see insets in Figure 1C,F). Though the curvature of the bowl wall is different due to the variation in annealing time, it has little effect on the shape of the ring structures as shown in Figure 1A,D,E. The final calcination at 400 °C does not destroy the ring structure; it only changes the crystal phase of the material.

A higher precursor concentration introduces more solute and, hence, leads to rings with larger outer diameter, higher height, and thicker walls. A longer annealing time increases the inner diameter of the ring arrays. Figure 4A,B shows the profile images of the colloidal monolayer annealed for 5 and 35 min, respectively. With a longer annealing time, contact areas increase and the inner diameter of the rings grows larger. At the same time, the interstices in the colloidal monolayer shrink during annealing, and hence fewer precursor molecules are available. This is why the walls become thinner after prolonged annealing. The annealing time and the precursor concentration should be confined in a certain range to ensure that there is continuous space between the colloidal monolayer and the substrate, where the precursor can be separated. For colloidal monolayers constructed with 4.5 μm PSs, the appropriate annealing time is 3−40 min, and the precursor concentration can be 0.005−0.2 M. An alternative means of controlling the ring size is by changing the sizes of PSs. For example, in Figure 5, the ring arrays were acquired by taking the 1 and 2 μm PS colloidal monolayers as templates.

The porous structures in the ring walls are perfect nanoconfined reactors for loading specific functional nanoparticles. We used a recently developed sono- and photochemical approach to deposit noble metal particles into the nanopores of TiO_2.[35] The procedure involved flushing the samples with deionized water to remove the noble metal precursor solution that did not enter the pores. After UV irradiation, the metal ions trapped in the pores were reduced to nanoparticles and coupled to TiO_2. As shown in Figure 6, the particle-loaded ring arrays possess very different optical absorption properties. The silver-loaded and gold-loaded rings show optical absorption peaks at 430 and 540 nm, respectively, while the pure nanoporous TiO_2 rings do not absorb visible light. Such optical functionalized rings may find applications in optoelectronic nanodevices.

Our methods can fabricate ring arrays on both flat and nonflat solid surfaces. The synthesis of ring arrays on curved surfaces involved two steps. First, a colloidal monolayer on the glass slide was transferred onto a corresponding curved substrate as in previous report.[32] The subsequent procedure was the same as the synthesis of ring arrays on the flat surface. Figure 7A,B are TiO_2 ring arrays on a concave

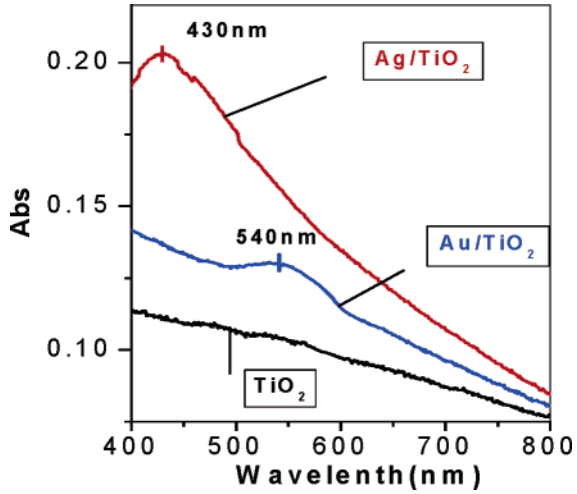

Figure 6. Optical absorption of nanoporous TiO_2, Au/TiO_2, and Ag/TiO_2 ring arrays.

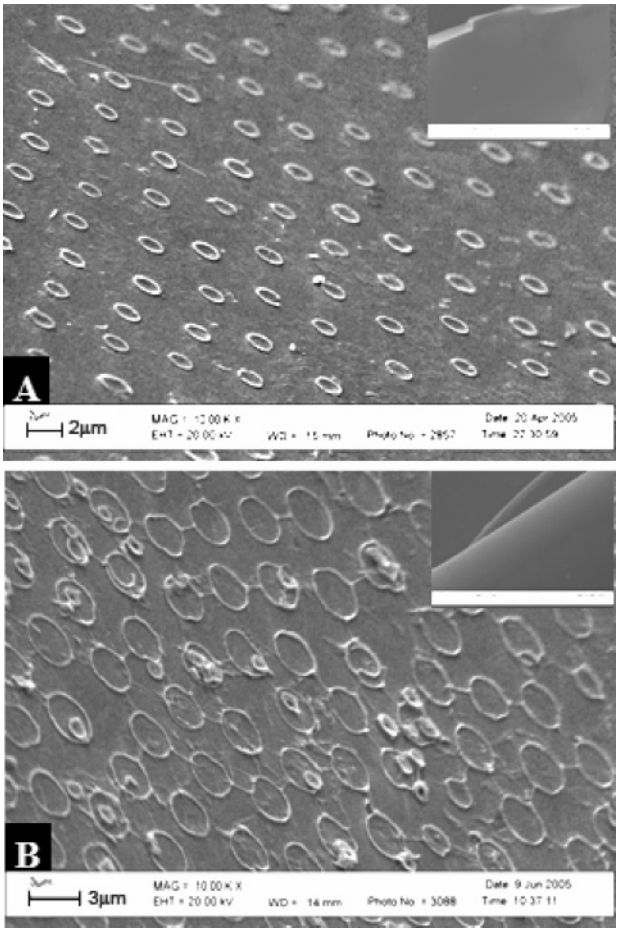

Figure 7. SEM images of TiO_2 ring arrays on a concave surface (A) and a convex surface (B). The precursor concentration was 0.1 M, and the annealing times were 5 and 25 min, respectively. The diameter of the PSs was 4.5 μm. The insets show the low-magnification images of the corresponding surfaces.

surface (inner surface of a glass tube) and a convex surface (outer surface of a glass tube), respectively. All the synthesis conditions for the two samples are the same as the samples shown in Figure 1A,E. The curvature radii (>0.5 mm) for the substrates in this study are two orders of magnitude larger than the sizes of the PSs (4.5 mm). Therefore, changes in the organization of PSs due to the irregular substrate geometry are negligible. As a result, the morphologies and controllability of the rings are virtually the same comparing to that on a flat substrate. This method obviously overcomes the restrictions of surface morphology.

Finally, it should be pointed out that the new nanoporous TiO_2 ring arrays might be an ideal material for gas sensors. TiO_2 by itself has been used as a gas-sensing material.[38] The porous wall structure can obviously enhance the diffusion of gaseous molecules and increase the sensitivity, and the highly ordered arrangement of rings should make such a sensor reproducible.[32] The sensor selectivity can be further improved by incorporating specific nanoparticles into the pores. Moreover, a novel magnetic data storage device may be constructed by filling the nanopores with magnetic particles.[39] The storage density per unit area is governed by the ring number which can be easily controlled by using templates of different sizes.[40,41] These potentials may be worth exploring.

Conclusions

In summary, using the annealed template-induced sol-soaking strategy, we were able to synthesize hierarchical nanoporous TiO_2 mesoscopic ring arrays on solid substrates. The ring formation was mainly based on the sol film rupturing confined in the specific microspaces between the colloidal monolayer and the substrate. The ring size can be systemically controlled by the annealing time of the PSs and the sol concentration without changing the CTC spacing between adjacent rings. Nanoporous structures are formed in the ring walls during gelling. This makes it easy to modify the ring arrays by incorporating specific functional particles into the pores. The rings can overcome the restrictions of surface morphology and grow on any solid support. Our preliminary study shows that other mesoscopic ring arrays including ZrO_2, SnO_2, Fe_2O_3, and ZnO can also be synthesized from appropriate precursors. These rings may find applications in photoelectric devices,[30] photocatalytic surfaces, magnetic elements, and gas sensors.

Acknowledgment. This work was supported by the Research Grants Council of the Hong Kong Special Administrative Region (Project No. 402904) and a Strategic Investments Scheme administrated by The Chinese University of Hong Kong.

Supporting Information Available: SEM image of 4.5 μm PS colloidal monolayer, large area SEM image of the ring array, and XRD pattern (PDF). This material is available free of charge via the Internet at http://pubs.acs.org.

CM060982S

(38) Rothschild, A.; Edelman, F.; Komen, Y.; Cosandey, F. *Sens. Actuators, B* **2000**, *67*, 282−289.
(39) Sort, J.; Glaczynska, H.; Ebels, U.; Dieny B.; Giersig, M.; Rybczynski, J. *J. Appl. Phys.* **2004**, *11*, 7516−7518.
(40) Sun, F. Q.; Cai, W. P.; Li, Y.; Duan, G. T.; Nichols, W. T.; Liang, C. H.; Koshizaki, N.; Fang, Q.; Boyd, W. I. *Appl. Phys. B* **2005**, *81*, 765−768.
(41) Haynes, C. L.; Van Duyne, R. P. *J. Phys. Chem. B* **2001**, *105*, 5599−5611.